J Nanostruct Chem (2014) 4:90
DOI 10.1007/s40097-014-0090-5

ORIGINAL

Zeolite–sepiolite nanoheterostructures

Almudena Gómez-Avilés · Carolina Belver · Pilar Aranda · Eduardo Ruiz-Hitzky · Miguel A. Camblor

Received: 24 January 2014 / Accepted: 17 February 2014 / Published online: 14 March 2014

Abstract Zeolite–sepiolite inorganic nanoheterostructures have been hydrothermally synthesized by adding a dispersion of colloidal sepiolite to a solution able to produce a nanocrystalline zeolite (silicalite). The obtained product could be recovered in good yield by simple filtration only when the relative sepiolite concentration exceeded a threshold of 1.8 wt% in the synthesis mixture (amounting to 1:3 sepiolite:zeolite wt. ratio in the recovered product). The resulting heterostructures were characterized by XRD, FTIR, thermal (TG–DTA) and chemical analyses, N_2 adsorption, TEM, SEM, ^{29}Si NMR, and methylene blue adsorption. The intimate zeolite–sepiolite interaction at the surface produced a good dispersion of zeolite particles and prevented their sintering upon calcination to remove the organic structure-directing agent. Experiments in conditions yielding microcrystalline silicalite support the idea that the sepiolite surface acts as nucleation sites for the zeolite crystallization. The textural properties of the nanozeolite–sepiolite heterostructure are not a linear combination of their components'.

Electronic supplementary material The online version of this article (doi:10.1007/s40097-014-0090-5) contains supplementary material, which is available to authorized users.

A. Gómez-Avilés · P. Aranda · E. Ruiz-Hitzky · M. A. Camblor (✉)
Instituto de Ciencia de Materiales de Madrid (ICMM), Consejo Superior de Investigaciones Científicas (CSIC), Sor Juana Inés de la Cruz 3, 28049 Madrid, Spain
e-mail: macamblor@icmm.csic.es

Present Address:
C. Belver
Departamento de Química Física Aplicada, Facultad de Ciencias, Universidad Autónoma de Madrid, Francisco Tomás y Valiente 7, 28049 Madrid, Spain

Keywords Zeolites · Sepiolite · Heterostructure · Nanoscale · Stability · Hydrothermal synthesis

Introduction

Heterostructures, i.e., systems in which different materials meet at the interfaces, have been attracting considerable attention because of the possibilities offered for tailoring the properties of the system [1]. On one hand, the properties of both components may be coupled in the resulting material. On the other hand, a strong interaction at the interface may result in modified properties, adding potential to this synthetic strategy for the development of new functional materials. Organic–inorganic, [2, 3] organic–organic, [4, 5] as well as inorganic–inorganic heterostructures, [6, 7] recently including silica-sepiolite nanostructures, [8] have been reported. When the controlled arrangement of nanoscale structural units affords "a configuration that creates a novel functionality through mutual interactions among those units" the approach is termed "nanoarchitectonics" [9–11]. Within these systems, several clay-based nanoarchitectures of interest for adsorption and catalysis processes have been developed [12]. Combining the swelling ability of organoclays with sol–gel procedures using silicon and diverse metal alkoxides resulted in a new route for the preparation of new porous nanoarchitectures [13]. In this way, swelling 2:1 layered silicates originate delaminated materials combined at the nanometric level with oxide nanoparticles resulting from the hydrolyzed alkoxides [3, 6, 14–16]. This route applied to fibrous clays, such as sepiolite, give rise to nanoarchitectures formed by individual nanoparticles assembled to the fibers surface [7, 8, 17]. Potential applications of heterostructures and nanoarchitectures may

include acid catalysis, photocatalysis, nanofillers for polymer reinforcement, etc.

Here, we report on a zeolite–sepiolite heterostructure, which combines at the nanoscale two phases with different chemical composition, different crystalline structure, and different textural properties and morphology. Both are nanocrystalline materials but the zeolite is so in any dimension, while sepiolite is nanocrystalline in only two dimensions.

Sepiolite is a natural fibrous hydrated magnesium silicate with ideal unit cell formula $[Si_{12}O_{30}Mg_8(OH,F)_4](H_2O)_4{\cdot}8H_2O$ [18, 19]. It crystallizes in the form of long needles (2-10 μm long by some 100-300 nm wide) and its crystal structure is composed of blocks encompassing structural tunnels with 11x4 $Å^2$ cross-section [18, 20]. Its relatively high specific surface area and strong mechanical and chemical stability makes sepiolite useful as adsorbent for organic compounds, like oils, and for organic and inorganic cations and also as support of catalysts and as nanofillers of diverse polymers [21, 22].

On the other hand, silica-based zeolites are natural or synthetic crystalline tectosilicates with structural pores and cavities and whose properties render them useful materials in a wide range of applications [23, 24]. Typically, these properties include cation exchange ability, a large surface area, the ability to adsorb gases in a confined space, and the possibility to introduce active catalytic sites. The wide chemical and structural diversity displayed by zeolites, particularly synthetic zeolites, add a large variety to their properties and applications [25]. One of the most studied and useful zeolites is ZSM-5, [26, 27] with a Zeolite Framework Type coded MFI [28]. It may be synthesized in pure silica form, receiving then the name "silicalite" [29, 30]. Several zeolites have been synthesized in nanocrystalline form, [31–37] providing better access to active sites inside their pores and a shorter intracrystalline path, both characteristics being of interest when processing large molecules and when the possibility of consecutive reactions may lower the selectivity to the desired products (as is the case, for instance, in the important fluid catalytic cracking, where heavy molecular weight fractions of crude oil are converted to lighter molecules for the production of high-quality fuels) [38].

Experimental

Materials preparation

The preparation of nanozeolite/sepiolite heterostructures was based on a modification of a previously reported procedure for the synthesis of nanocrystalline silicalite-1 starting from a clear homogeneous solution [34]. First, a given amount of a rheological grade sepiolite (PANGEL *S*9, >95% distributed by TOLSA) [39] was suspended in water with stirring. Then, tetraethoxysilane (TEOS, Aldrich), tetrapropylammonium hydroxide (TPAOH, 1.0 M aqueous solution in water, Sigma-Aldrich), and NaOH (Puriss. p.a., Fluka) were added to attain the molar composition 9 TPAOH : 0.2 NaOH : 25 SiO_2: 880 H_2O : 100 EtOH (where EtOH stands for the ethanol released by TEOS upon hydrolysis, which was not allowed to evaporate). The obtained mixtures (clear, transparent and colorless in the absence of sepiolite and light brown in its presence) were introduced in capped polypropylene bottles and allowed to homogenize for 16 hours under magnetic stirring at RT. All the gels became whitish at that point. After transferring the mixtures to Teflon-lined autoclaves, they were heated under autogenous pressure for 30 h at 100 °C either statically or while tumbling the autoclave at 60 rpm. The obtained nanozeolite/sepiolite solids were filtered with a Millipore membrane with 0.45 μm pore size (Type HVLP Durapore® polyvinylidene difluoride). In the case of the sepiolite-free zeolite, the product was recovered by centrifugation (10,200 r.p.m. for 15 min., see below). In all cases, the resulting materials were washed several times with double-distilled water up to achieving a $pH < 10$ in the waste liquid and then dried at 60 °C. The structure-directing agent was removed by calcination in air at 600 °C for 5 h to produce the micro-mesoporous heterostructures. Samples with different contents of sepiolite were produced (Table 1).

Table 1 Sepiolite content of the different synthesis mixtures and yield of recovered solids (wt%)

Sample	Sepiolite In gel	Solid Yield	Zeolite Yield[a]	Sepiolite In solid[a]
nMFI	0	4.0[b]	4.0	0.0
nMFIsep1	0.37	2.7[c]	2.3	13.6
nMFIsep2	1.11	6.2[c]	5.2	17.7
nMFIsep3	1.85	7.2	5.4	25.4
nMFIsep4[d]	1.86	7.2	5.4	25.5

[a] assuming sepiolite is fully recovered in the solid. [b] solid recovered by centrifugation (all the other recovered by filtration). [c] whitish filtrate. [d] the autoclave was tumbled at 60 rpm during the crystallization. The rest of samples was heated statically

Characterization

X-ray diffraction (XRD) profiles of the samples were recorded on a Bruker D8 diffractometer working at 40 kV and 30 mA and employing Ni-filtered Cu K_α radiation. FTIR spectra were recorded in two different equipments, on a NICOLET 20SXC and on a BRUKER ISS 66V-S, using the KBr technique (2 wt% sample concentration,

pelletized at 10 Ton) in the 4000–400 cm^{-1} range. Field Emission Scanning Electron Microscopy (FE-SEM) was performed on uncoated samples using a FEI microscope Nova NanoSEM 230 model. Transmission Electron Microscopy (TEM) measurements were carried out on a STEM-LEO 910 microscope, operating at 80 kV. The samples were dispersed in an aqueous suspension and transferred directly on a 200 mesh copper grid covered with carbon. Thermoanalyses were carried out in a SEIKO SSC/5200 thermogravimetric/differential thermal analysis (TG/DTA) instrument. The samples (10–20 mg) were heated from room temperature to 1000 °C at a heating rate of 5 or 10 °C min^{-1} under dynamic air. The ^{29}Si solid-state MAS NMR spectra at 79.49 MHz were acquired on a Bruker AV-400-WB spectrometer equipped with a 4 mm MAS NMR probe, with the samples spinning at a rate of approximately 10 kHz and using a π/12 pulse of 5.0 μs and 5.0 s recycle delay. $^{29}Si\{^{1}H\}$ CPMAS NMR spectra were obtained in the same equipment using a contact time of 6 ms. Chemical shifts are referenced to tetramethylsilane (TMS) at $\delta = 0$ ppm. Textural properties were analyzed by N_2 adsorption/desorption isotherms performed at −196 °C using a static volumetric apparatus, Micromeritics ASAP 2010 instrument. Before the analysis, the samples (150–200 mg) were outgassed at 150 °C, overnight or till the outgassing pressure reached 5 mmHg. The specific total surface area was calculated using the Brunauer–Emmett–Teller (BET) method, [40] using the adsorption data in the 0.05-0.2 P/P_0 range, adjusting the C value from 50 to 150, [41] and considering a nitrogen molecule cross-section of 0.162 nm^2 [42]. The external surface area (S_{ext}) and micropore volume (V_{mic}) were obtained by means of the t-plot according to De Boers method[43]. The total pore volume (V_p) of the solids was estimated from the amount of nitrogen adsorbed at a relative pressure of 0.99, assuming that the density of the nitrogen condensed in the pores is equal to that of liquid nitrogen at −196 °C, i.e. 0.81 g cm^{-3} [42]. Adsorption of cationic dyes: Methylene blue (MB) was used as a model cationic dye to evaluate the adsorption behavior of the zeolite/sepiolite heterostructures. 200 mg of sample was placed in a vial containing 25 ml of organic dye solutions of known mass concentration (5.12 ppm). The solution was magnetically stirred for 30 min at 25 °C. Following adsorption, the samples were centrifuged with a Millipore membrane (0.45 μm pore size) and washed several times with double-distilled water. The dye concentration remaining in the supernatant was analyzed spectrophotometrically using a double beam UV–VIS spectrophotometer (Varian, UV–VIS Spectrometer, Cary 100) by measuring the absorbance at λ_{max} of 664 nm and also by CHNS chemical analysis performed in a LECO CHNS-932 or a PERKIN-ELMER 2400.

Results and discussion

The nanocrystalline MFI prepared in the absence of sepiolite could not be filtered, as all the solid passed the filter, and had to be recovered by centrifugation, as noted in the experimental section. Washing this zeolite also required successive centrifugation steps. By contrast, the solids that contained sepiolite could be recovered by filtration although with different levels of efficiency, as shown in Table 1. For the experiment with the smallest sepiolite content, 0.37 %, a whitish filtrate suggested some zeolite product still passed the filter and the amount of solids recovered was roughly half of the amount recovered in the experiments with the highest sepiolite content. Interestingly, increasing the sepiolite content in the synthesis mixture to 1.11 % yielded a more transparent filtrate, although still slightly whitish, and allowed to recover almost the maximum amount of zeolite, actually more than obtained by centrifugation in the sepiolite-free experiment. For higher sepiolite contents, a transparent and colorless filtrate with maximum solid yield revealed the complete retention of the zeolite product in the filter. The yield of zeolite recovered increased from 35 (nMFIsep1) up to 83 g of zeolite per 100 g of SiO_2 (nMFIsep3 and nMFIsep4), surpassing the 61 % obtained by centrifugation of the sepiolite-free synthesis.

This is obviously an interesting feature of the synthesis method reported here since, typically, nanocrystalline zeolites need to be recovered by long centrifugation at high speed. It could be argued that sepiolite functions here as a mere filter aid. However, when sepiolite was mixed under stirring with a zeolite synthesis gel already treated at 100 °C for 30 h, all the zeolite passed the filter, showing that the mere presence of sepiolite is not able to retain the nanocrystals and sepiolite does not act as a simple filter aid. Rather, we contend that there is an intimate interaction between zeolite nanocrystals and the sepiolite fibers. In support to this idea, we have observed that sepiolite acts as a promoter for the nucleation of silicalite with a large crystal size (see Additional file 1), and in the case of the nanosilicalite described here, this promotion effect explains the slightly larger crystal size obtained in the presence of sepiolite (see below) and the total retention on the paper filter. For the experiments with the smaller sepiolite contents, it is likely that the sepiolite surface available for interaction with the zeolite is not as large as needed to retain the whole zeolitic product.

The XRD patterns of untreated sepiolite, as-made nMFI, and the as-made nMFIsep heterostructures are shown in Fig. 1. All the zeolite-containing samples showed the characteristic pattern of zeolite MFI and the heterostructures also showed the characteristic (110) reflection of sepiolite around 1.23 nm (JCPDS data No. 130595). This

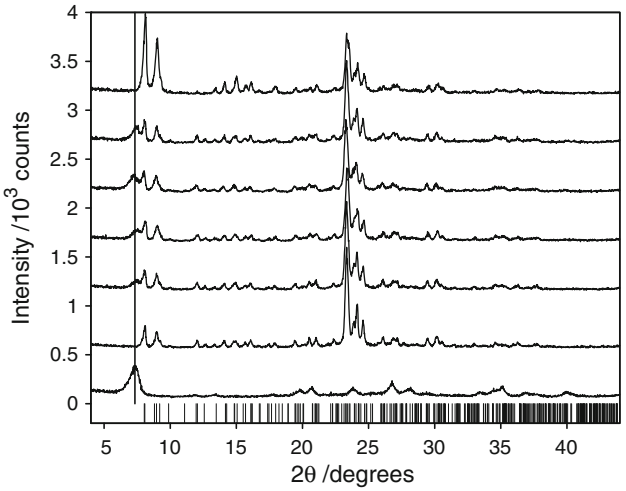

Fig. 1 XRD patterns for (*bottom to top*) sepiolite and as-made nMFI, nMFIsep1, nMFIsep2, nMFIsep3, nMFIsep4 and calcined nMFIsep4. *Short vertical lines* mark allowed reflections for MFI in space group Pnma. The *long vertical line* marks the position of the (100) reflection of sepiolite

suggests the crystal structure of sepiolite is not substantially affected by the treatment, despite the high pH. To better ascertain this conclusion, sepiolite was treated in the same conditions but without addition of TEOS, to avoid zeolite crystallization. After the treatment, the XRD pattern of sepiolite was essentially unaltered (see Additional file 2), suggesting the sodium level in the reaction mixture is too low to afford the formation of a loughlinite-type derivative (for this, the first reflection should have moved some 0.5 ° to lower angles) [44].

After calcination at 600 °C, no signs of sepiolite were observed by XRD, even for the material with the highest sepiolite content (over 25% sepiolite in nMFIsep4, see Fig. 1, top). This is not unexpected because sepiolite changes its structure upon heating above 400 °C. The so-called "zeolitic water" is lost below 300 °C without significant structural changes, while coordinated water is removed at 400–600 °C, with crystal folding occurring near 500 °C [20, 45–48]. This folding results in a lost of microporosity and the disappearance of the intense (110) sepiolite reflection, with new reflections appearing with much lower intensity in the 8°–10° 2θ region, where they are masked by the very strong reflections of the calcined zeolite (see Additional file 3). Sepiolite folding, with the concomitant loss of microporosity, becomes irreversible after thermal treatments above 500 °C [21].

The FE-SEM images of the pure zeolite and of the heterostructures (Fig. 2) reveal that all the zeolite materials are nanocrystalline, with rather uniform crystal sizes of around 100 nm in the absence of sepiolite and closer to around 160 nm in its presence. There are not significant changes in morphology when the zeolite crystallizes in the presence of sepiolite and no changes in the morphology of sepiolite itself by the hydrothermal or calcination treatments, as expected. It is noticeable, however, that in the pure zeolite, the crystals appear to be quite compactly aggregated, while the heterostructures look less dense and more spongy. This is specially clear for the calcined materials where the FE-SEM images reveal necks in crystal–crystal contacts in the zeolite prepared in the absence of sepiolite, suggesting sintering of the nanocrystals. That sintering occurs in the nMFI but not in the nMFIsep4 material may be actually due to the smaller crystal size of the former, because calcination of a micron-sized MFI zeolite (around 20 μm, synthesized by the method reported by Feoktistova et al. [49]) up to 1,000 °C showed a remarkable stability, with no signs of degradation that could be observed by SEM or XRD. The nMFIsep4 sample, which was synthesized under the same conditions as nMFIsep3 but while tumbling the autoclaves during thermal treatment, showed only a marginally better dispersion of the zeolite crystals on the sepiolite fibers.

To further investigate the issue of sintering, two samples calcined at 600 °C (nMFI and nMFIsep4, i.e. with no sepiolite and with the highest sepiolite content, respectively) were chosen for TEM analysis (Fig. 3). The results show that, in the absence of sepiolite, the zeolite forms compact aggregates of crystals in close contact with the surrounding zeolite crystals (sintering is less visible in transmission mode). There are also lighter contrast spots, suggesting areas of lower electron density and, hence, some structural damage occurred during calcination. By contrast, in the sepiolite containing sample, the zeolite crystals are largely dispersed, rather separated from each other, and in close contact with the sepiolite fibers. In fact, we have found no zeolite crystallite isolated from a sepiolite fiber and no lighter spots associated to structural damage. Since these images correspond to calcined materials (see more TEM images in Additional file 4), the zeolite–sepiolite association has been strong enough to prevent agglomeration of the zeolite crystals, with zeolite–sepiolite associations dominating, while in the absence of zeolite not just aggregation but also sintering occurred (although this may be due to the smaller crystal size, see above). The zeolite dispersion in the sepiolite matrix may prevent structural damage during calcination, as heat can dissipate more effectively and organic residues may be more easily removed. This is corroborated by TG-DTA measurements that show that the main weight loss associated with the exothermic removal of organics occurs at a lower temperature in nMFIsep4 than in nMFI (maxima in ATD at 344 and 369 °C, respectively, see Additional file 5), despite the slightly larger crystal size of the zeolite in nMFIsep4.

The ^{29}Si MAS NMR and $^{29}Si\{^{1}H\}$ CP MAS NMR spectra of nMFIsep4 before and after calcination are shown

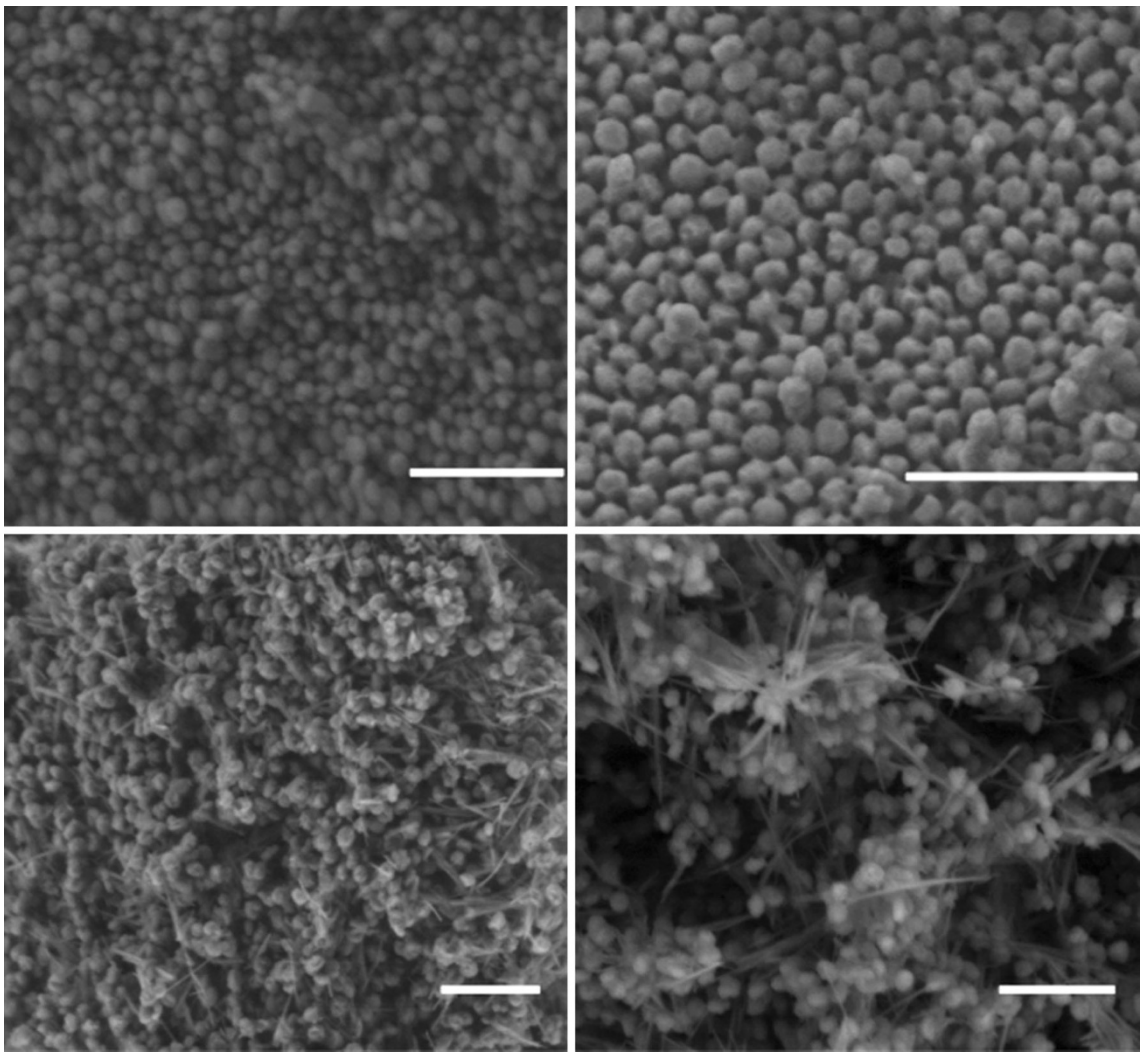

Fig. 2 FE-SEM images of as-made (*left*) and calcined (*right*) nanosilicalite synthesized in the absence (*top*) and in the presence of sepiolite (nMFIsep4, *bottom*). *Scale bars* 1 μm

in Fig. 4. Before calcination, the three resonances characteristic of sepiolite are observed at ca. −93, −95, and −99 ppm, corresponding to the three Q^3 crystallographic sites in sepiolite [50]. All the tetrahedra in the silicate layer of sepiolite are Q^3, as they are coordinated to three neighbor tetrahedra, while the fourth O is shared by three Mg atoms in the octahedral layer [51]. The zeolite signals are barely seen due to the short recycle delay used and the characteristically long spin-lattice relaxation time observed in as-made high-silica zeolites [52, 53]. The $^{29}Si\{^1H\}$CP MAS NMR spectrum has a much better signal-to-noise ratio and the Q^3 signals of sepiolite are much better resolved. Also, the resonances due to Si in the zeolite are clearly observed: the Q^3 signal at −103 ppm, indicative of silanol and/or silanolate groups arising from connectivity defects and the broad and asymmetric Q^4 resonance around −113 ppm. Upon calcination, the ^{29}Si MAS NMR spectrum has an improved signal-to-noise ratio, a lower concentration of zeolitic Q^3 defects sites in the zeolite and a broad and blurred resonance at the spectral region corresponding to the sepiolite Q^3 resonances. High and pure silica zeolites synthesized at high pH typically have a large concentration of connectivity defects that are annealed, at least partially, upon calcination[54]. Cross polarization to ^{1}H in this case does not improve the spectrum: while the zeolite resonances mainly disappeared because of the lack of close H–Si interactions in this hydrophobic material, the Q^3 region of sepiolite is still broad and essentially featureless, suggesting significant structural collapse, as already discussed above.

The infrared spectra of nMFI and of the heterostructures are shown in Fig. 5. The spectra of the heterostructures are largely dominated by the zeolite vibrational bands, which overlap and mask the sepiolite bands. Only at the highest

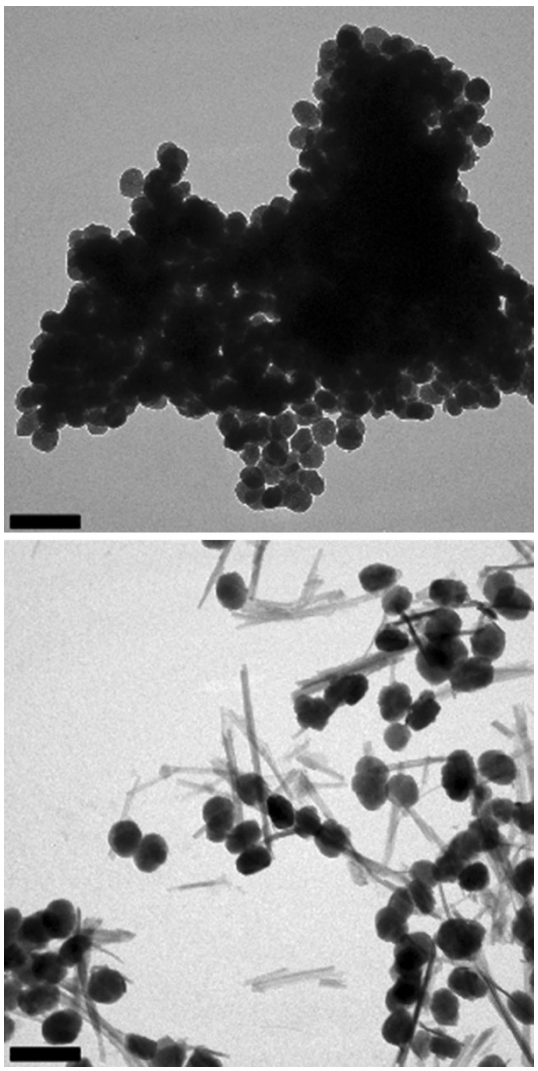

Fig. 3 TEM images of calcined nMFI (*top*) and calcined nMFIsep4 (*bottom*). *Scale bars* 0.4 μm

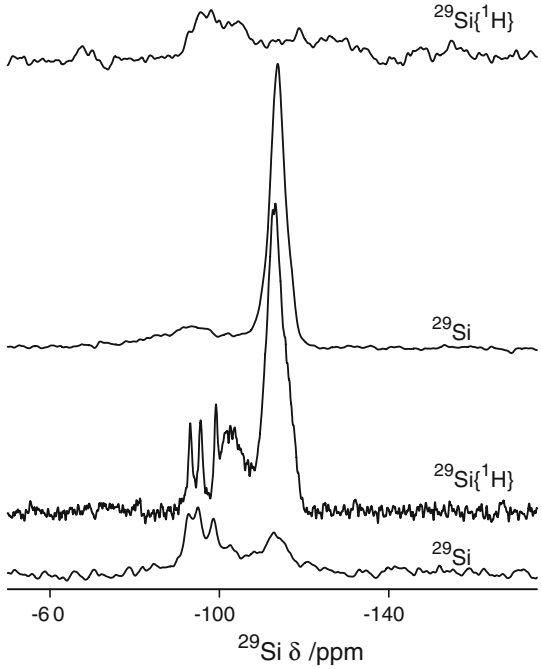

Fig. 4 ^{29}Si NMR spectra of (*from bottom to top*): as-made (^{29}Si and $^{29}Si\{^{1}H\}$ CP) and calcined nMFIsep4 (^{29}Si and $^{29}Si\{^{1}H\}$ CP)

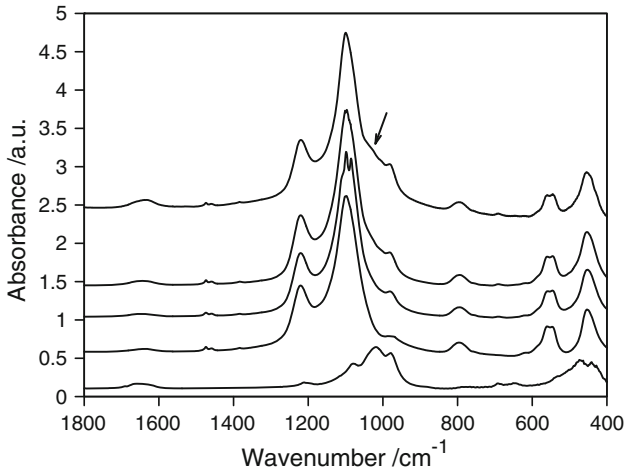

Fig. 5 Infrared spectra of (*from bottom to top*): sepiolite and as-made nMFI, nMFIsep1, nMFIsep2, nMFIsep4. The *arrow* points to the 1,020 cm^{-1} Si–O–Si in-plane vibration of sepiolite showing up in the heterostructures with larger sepiolite contents. Absorbance given in absorbance units

sepiolite content, a broad shoulder around 1,020 cm^{-1} assigned to Si–O–Si in-plane vibrations in sepiolite becomes clearly discernible [48]. A small and broad band around 970-980 cm^{-1} in nMFI, assigned to the stretching vibration of Si–O polarized bonds, [55] including Si–OH or Si–O^{-}, [56–58] becomes sharper in the heterostructures, possibly by overlapping with the 977 cm^{-1} band of sepiolite. After calcination, this band almost disappears in the pure zeolite, while the heterostructure shows a band in the same region that can be attributed to the calcined sepiolite (Fig. 6).

The textural properties of the heterostructures, collected in Table 2, have been investigated by N_2 adsorption/desorption isotherms at −196 °C. Before calcination (Fig. 7), sepiolite and nMFI both show non-reversible type IIb isotherms, with a H3 hysteresis loop, characteristic of powders or aggregates, where the particles arrangement generates non-rigid porous in the inter-particle space [42]. By contrast, nMFIsep4 shows a much narrower hysteresis loop, being an isotherm almost reversible of type IIa [42]. This kind of isotherm is common for an open and stable surface that suffers a normal monolayer-mutilayer adsorption. The almost complete lack of hysteresis in nMFIsep4, despite its presence in its pure constituents, suggests that, on one hand, the dispersion of the zeolite in

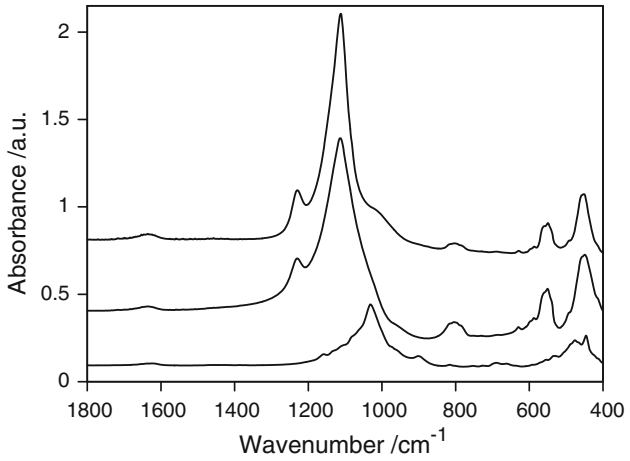

Fig. 6 Infrared spectra of (*from bottom to top*): sepiolite, nMFI and nMFIsep4 after calcination at 600 °C for 5 h. Absorbance given in absorbance units

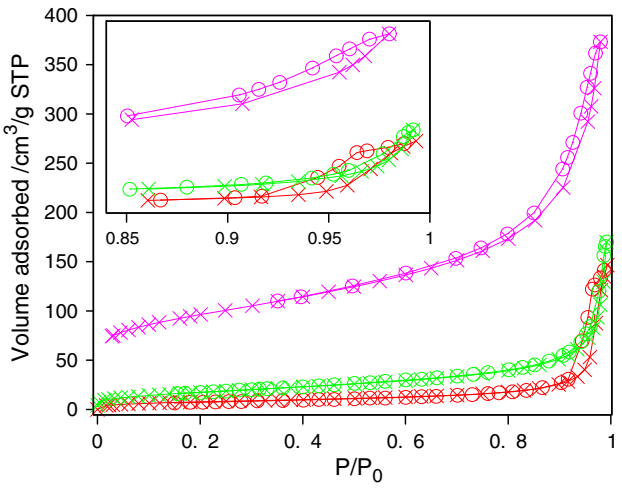

Fig. 7 N_2 adsorption (x) and desorption (^) isotherms at −196°C for untreated sepiolite (*pink*), nMFI (*red*) and nMFIsep4 (*green*). The inset shows the 0.85–1 relative pressure range

Table 2 Textural properties of sepiolite, nMFI and the nMFIsep4 heterostructure before and after calcination at 600 °C

Sample	S_{BET}	S_μ	S_{Ext}	V_μ	V_T
Sepiolite	344	123	221	0.05	0.58
Sepiolite Calc.	138	2	136	0.00	0.51
nMFI	28	1	27	0.00	0.21
nMFI Calc.	282	237	45	0.12	0.43
nMFIsep4	63	0	63	0.00	0.20
nMFIsep4 Calc.	306	204	102	0.10	0.37

S_{BET}, S_μ and S_{Ext} are, respectively, surface area determined by the BET method, microporous surface determined by the t-plot method and external surface determined by difference, and are given in $m^2 g^{-1}$. V_μ and V_T are micropore volumes determined by the t-plot method and total pore volume at the highest relative pressure, and are given in $cm^3 g^{-1}$

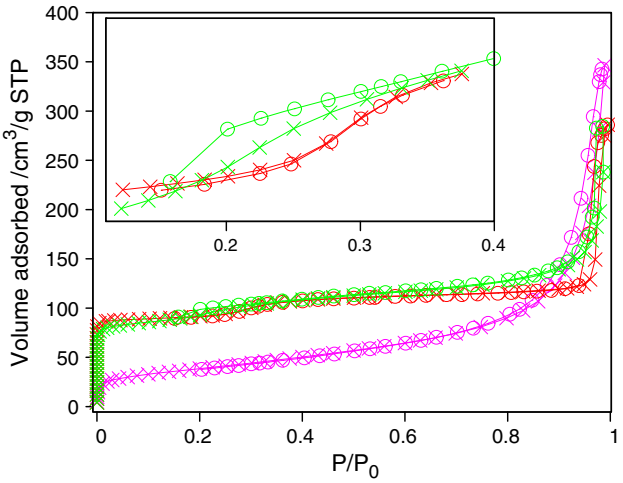

Fig. 8 N_2 adsorption (x) and desorption (°) isotherms at −196 °C for sepiolite (*pink*), nMFI (*red*) and nMFIsep4 (*green*) after calcination at 600 °C. The inset shows the step in the isotherms of nMFI and nMFIsep4, in the 0.1–0.4 relative pressure range

the heterostructure prevents the formation of inter-particle pores between zeolite particles. On the other hand, the intercrystal pore space inside sepiolite microfibers may be blocked by adsorption of TPA. Both nMFI and nMFIsep4 have poor textural properties, low N_2 volume adsorbed, low surface area, and no microporosity, because the zeolite pores are blocked by the organic structure-directing agent (TPA) still occluded in the pores. After calcination at 600 °C, sepiolite looses its microporosity, as a consequence of crystal folding, as explained above, while nMFI and nMFIsep4 become microporous (Fig. 8). Both calcined nMFI and nMFIsep4 show an isotherm close to Type I with a step typical of N_2 adsorption in high-silica MFI, which is ascribed to a phase transition in the adsorbate phase [59]. Interestingly, the step is similar in size for nMFI and nMFIsep4, while it starts at a lower relative pressure in nMFIsep4. In addition, nMFIsep4 now displays a small hysteresis loop likely associated to the loss of TPA adsorbed inside the sepiolite fibers. Also of interest, the total BET area, micropore area and volume, and external surface area of the calcined heterostructure are larger than expected for its 75:25 zeolite:sepiolite constituents weight ratio, considering the loss of microporosity of sepiolite calcined at 600 °C. This may likely be due to the lack of sintering and structural damage in the heterostructure.

A potential application for sepiolite–zeolite heterostructures is the removal of organic molecules from waste waters. The adsorption capacity of sepiolite could be combined with the catalytic activity of the zeolite, after introduction of a catalytic function by, for instance,

isomorphous substitution of Si by Al or Ti, respectively, for the efficient removal of contaminants. Thus, we have studied the properties of the heterostructures as adsorbents for organic molecules using methylene blue. The calcined sepiolite and nMFI adsorbed 14.7 and 3.8 moles MB per 100g, respectively, while the calcined nMFIsep4 heterostructure adsorbs 7.7 moles/100g. This is slightly above the expected value for a physical mixture of 75:25 g sepiolite:zeolite (6.5 moles/100g), which again may be due to the lack of zeolite sintering in the heterostructure. The loss of microporosity of calcined sepiolite is, in this case, not detrimental, since MB is too large to be adsorbed inside the sepiolite channels [20].

Conclusions

We have prepared silicalite-sepiolite heterostructures with an intimate interaction between both nanocrystalline moieties, which is likely due to the nucleation and growth of the nanozeolite on the surface of the sepiolite fibers. This interactions allow to fully recover and wash the nanozeolite material on paper filter, without recourse to long and tedious centrifugation steps. Calcination at 600 °C of a nanosilicalite prepared in the absence of sepiolite under otherwise identical conditions shows signs of structural damage (sintering between particles and lighter spots in TEM), which are not detected in the corresponding heterostructure. We attribute the effect mainly to a slight increase in the zeolite crystal size but also possibly to the dispersion of zeolite nanocrystals. The increased thermal stability provides improved textural properties in the final calcined material, despite the loss of microporosity in the calcined sepiolite.

Acknowledgements Financial support from the Spanish CICYT, MAT2012-31759, is acknowledged. C. Belver acknowledges MINECO for a "Ramon y Cajal" contract. We also thank A. Valera and F. Pinto for technical expertise (FE-SEM and TEM, respectively).

Conflict of interest The authors declare that they have no competing interests.

References

1. Zheng, H., Li, Y., Liu, H., Yin, X., Li, Y.: Construction of heterostructure materials toward functionality. Chem. Soc. Rev. **40**, 4506–4524 (2011)
2. Cincotti, S., Rabe, J.P.: Self-assembled alkane monolayers on MoSe2 and MoS2. Appl. Phys. Lett. **62**(26), 3531–3533 (1993)
3. Zapata, P.A., Belver, C., Quijada, R., Aranda, P., Ruiz-Hitzky, E.: Silica/clay organo-heterostructures to promote polyethylene-clay nanocomposites by *in situ* polymerization. Appl. Catal. A **453**, 142–150 (2013)
4. Simbrunner, C., Hernandez-Sosa, G., Quochi, F., Schwabegger, G., Botta, C., Oehzelt, M., Salzmann, I., Djuric, T., Neuhold, A., Resel, R., Saba, M., Mura, A., Bongiovanni, G., Vollmer, A., Koch, N., Sitter, H.: Color tuning of nanofibers by periodic organic-organic hetero-epitaxy. ACS Nano. **6**(6), 4629–4638 (2012)
5. Hinderhofer, A., Schreiber, F.: Organic-organic heterostructures: concepts and applications. ChemPhysChem **13**(3), 628–643 (2012)
6. Letaïef, S., Ruiz-Hitzky, E.: Silica-clay nanocomposites. Chem. Commun. **24**, 2996–2997 (2003)
7. Belver, C., Aranda, P., Ruiz-Hitzky, E.: Silica-alumina/sepiolite nanoarchitectures. J. Mater. Chem. A **1**(25), 7477–7487 (2013)
8. Gomez-Avilés, A., Aranda, P., Fernandes, F.M., Belver, C., Ruiz-Hitzky, E.: Silica-sepiolite nanoarchitectures. J. Nanosci. Nanotechnol. **13**(4), 2897–2907 (2013)
9. Aono, M., Bando, Y., Ariga, K.: Nanoarchitectonics: Pioneering a new paradigm for nanotechnology in materials development. Adv. Mater. **24**(2), 150–151 (2012)
10. Ariga, K., Vinu, A., Yamauchi, Y., Ji, Q., Hill, J.P.: Nanoarchitectonics for mesoporous materials. B. Chem. Soc. Jpn. **85**(1), 1–32 (2012)
11. Ariga, K., Yamauchi, Y., Rydzek, G., Ji, Q., Yonamine, Y., Wu, K.C.-W., Hill, J.P.: Layer-by-layer nanoarchitectonics: invention, innovation, and evolution. Chem. Lett. **43**(1), 36–68 (2014)
12. Ruiz-Hitzky, E., Aranda, P., Belver, C.: Nanoarchitectures based on clay materials. In: Ariga, K. (ed.) Manipulation of nanoscale materials. An introduction to nanoarchitectonics. RSC nanoscience & nanotechnology, vol **24**, pp. 87–111. The Royal Society of Chemistry, Cambridge (2012)
13. Ruiz-Hitzky E., Aranda P.: Novel architectures in porous materials based on clays. (2014). doi:10.1007/s10971-013-3237-9
14. Letaïef, S., Martín-Luengo, M.A., Aranda, P., Ruiz-Hitzky, E.: A colloidal route for delamination of layered solids: Novel porous-clay nanocomposites. Adv. Funct. Mater. **16**(3), 401–409 (2006)
15. Manova, E., Aranda, P., Martín-Luengo, M.A., Letaïef, S., Ruiz-Hitzky, E.: New titania-clay nanostructured porous materials. Micropor. Mesopor. Mater. **131**(13), 252–260 (2010)
16. Belver, C., Aranda, P., Martín-Luengo, M.A., Ruiz-Hitzky, E.: New silica/alumina-clay heterostructures: properties as acid catalysts. Micropor. Mesopor. Mater. **147**(1), 157–166 (2012)
17. Aranda, P., Kun, R., Martín-Luengo, M.A., Letaïef, S., Dékány, I., Ruiz-Hitzky, E.: Titania-sepiolite nanocomposites prepared by a surfactant templating colloidal route. Chem. Mater. **20**(1), 84–91 (2008)
18. Brauner, K., Preisinger, A.: Miner. Petr. Mitt. **6**, 120–140 (1956)
19. Santaren, J., Sanz, J., Ruiz-Hitzky, E.: Structural fluorine in sepiolite. Clays Clay Miner. **38**, 63–68 (1990)
20. Ruiz-Hitzky, E.: Molecular access to intracrystalline tunnels of sepiolite. J. Mater. Chem. **11**(1), 86–91 (2001)
21. Alvarez, A., Santaren, J., Esteban-Cubillo, A., Aparicio, P.: In: Galán, E., Singer, A. (eds.) Developments in Palygorskite-Sepiolite Research. A New Outlook on These Nanomaterials, pp. 281–298. Elsevier, Amsterdam (2011). Chap. 12
22. Ruiz-Hitzky, E., Aranda, P., Alvarez, A., Santaren, J., Esteban-Cubillo, A.: In: Galán, E., Singer, A. (eds.) Developments in Palygorskite-Sepiolite Research. A New Outlook on These Nanomaterials, pp. 393–452. Elsevier, Amsterdam (2011). Chap. 17
23. Mumpton, F.A.: La roca magica: Uses of natural zeolites in agriculture and industry. Proc. Natl. Acad. Sci. USA **96**(7), 3463–3470 (1999)

24. Sherman, J.D.: Synthetic zeolites and other microporous oxide molecular sieves. Proc. Natl. Acad. Sci. USA **97**(11), 6236–6236 (2000)
25. Camblor, M.A., Hong, S.B.: In: Bruce, D.W., O'Hare, D., Walton, R.I. (eds.) Porous Materials. Inorganic Materials Series, pp. 265–325. Wiley, Chichester (2011)
26. Argauer, R.J., Landolt, G.R.: (1972) US Pat. 3,702,886
27. Olson, D.H., Kokotailo, G.T., Lawton, S.L., Meier, W.M.: Crystal structure and structure-related properties of ZSM-5. J. Phys. Chem. **85**(15), 2238–2243 (1981)
28. Baerlocher, C., McCusker, L.B.: Database of Zeolite structures. http://www.iza-structure.org/databases/ (2014). Accessed 21 Jan 2014
29. Grose, R.W., Flanigen, E.M.: (1977) US Pat. 4,061,724
30. Flanigen, E.M., Bennett, J.M., Grose, R.W., Cohen, J.P., Patton, R.L., Kirchner, R.M., Smith, J.V.: Silicalite, a new hydrophobic crystalline silica molecular sieve. Nature **271**(5645), 512–516 (1978)
31. Jacobs, P.A., Derouane, E.G., Weitkamp, J.: Evidence for X-ray-amorphous zeolites. J. Chem. Soc., Chem. Commun. (12), 591–593 (1981)
32. Schoeman, B.J., Sterte, J., Otterstedt, J.E.: Synthesis and size tailoring of colloidal zeolite particles. J. Chem. Soc., Chem. Commun. (12), 994–995 (1993)
33. Schoeman, B.J., Sterte, J., Otterstedt, J.E.: Colloidal zeolite suspensions. Zeolites **14**(2), 110–116 (1994)
34. Persson, A.E., Schoeman, B.J., Sterte, J., Otterstedt, J.E.: The synthesis of discrete colloidal particles of TPA-silicalite-1. Zeolites **14**(7), 557–567 (1994)
35. Persson, A.E., Schoeman, B.J., Sterte, J., Otterstedt, J.E.: Synthesis of stable suspensions of discrete colloidal zeolite (Na, TPA)ZSM-5 crystals. Zeolites **15**(7), 611–619 (1995)
36. Zhang, G., Sterte, J., Schoeman, B.: Discrete colloidal crystals of titanium silicalite-1. J. Chem. Soc., Chem. Commun. (22), 2259–2260 (1995)
37. Camblor, M.A., Corma, A., Mifsud, A., Perez-Pariente, J., Valencia, S.: Synthesis of nanocrystalline zeolite beta in the absence of alkali metal cations. Stud. Surf. Sci. Catal. **105**, 341–348 (1997)
38. Camblor, M.A., Corma, A., Martínez, A., Mocholí, F.A., Pérez-Pariente, J.: Catalytic cracking of gasoil. Benefits in activity and selectivity of small Y zeolite crystallites stabilized by a higher silicon-to-aluminium ratio by synthesis. Appl. Catal. **55**(1), 65–74 (1989)
39. Alvarez, A., Pérez, R., Aragon, J.J.: Esteban MA EP 170,299 (1986)
40. Brunauer, S., Emmett, P., Teller, E.: Adsorption of gases in multimolecular layers. J. Am. Chem. Soc. **60**, 309–319 (1938)
41. Sing, K.: The use of nitrogen adsorption for the characterisation of porous materials. Colloids Surf., A 187, 3-9 (2001). 2nd International TRI/Princeton Workshop on Characterization of Porous Materials, Princeton, NJ, JUN 19-21 (2000)
42. Rouquerol, J., Rouquerol, F., Llewellyn, P.L., Maurin, G., Sing, K.: Adsorption by Powders and Porous Solids. Principles, Methodology and Applications,. Academic Press, London (2013)
43. Lippens, B.C., deBoer, J.H.: Studies on pore systems in catalysts. V. The t method. J. Catal. **4**(3), 319–323 (1965)
44. Fahey, J.J., Ross, M., Axelrod, J.M.: Loughlinite, a new hydrous sodium magnesium silicate. Am. Mineral. **45**, 270–281 (1960)
45. Serna, C., Ahlrichs, J.L., Serratosa, J.M.: Folding in sepiolite crystals. Clays Clay Miner. **23**, 452–457 (1975)
46. Ruiz, R., del Moral, J.C., Pesquera, C., Benito, I., González, F.: Reversible folding in sepiolite: study by thermal and textural analysis. Thermochim. Acta **279**(0), 103–110 (1996)
47. Sandí, G., Winans, R.E., Seifert, S., Carrado, K.A.: In situ saxs studies of the structural changes of sepiolite clay and sepiolite-carbon composites with temperature. Chem. Mater. **14**, 739–742 (2002)
48. Perraki, T., Orfanoudaki, A.: Study of raw and thermally treated sepiolite from the Mantoudi area, Euboea, Greece. J. Therm. Anal. Calorim. **91**, 589–597 (2008)
49. Feoktistova, N.N., Zhdanov, S.P., Lutz ,W., Büllow, M.: On the kinetics of crystallization of silicalite I. Zeolites **9**(2), 136–139 (1989)
50. Weir, M.R., Kuang, W., Facey, G.A., Detellier, C.: Solid-state nuclear magnetic resonance study of sepiolite and partially dehydrated sepiolite. Clays Clay Miner. **50**(2), 240–247 (2002)
51. Post, J.E., Bish, .DL., Heaney, P.J.: Synchrotron powder X-ray diffraction study of the structure and dehydration behaviour of sepiolite. Am. Miner. **92**, 91–97 (2007)
52. Klinowski, J., Carpenter, T.A., Thomas, J.M.: The origin of ^{29}Si spin-lattice relaxation in zeolites: a means of rapid acquisition of NMR spectra and of probing internal sites in microporous catalysts. J. Chem. Soc., Chem. Commun. (12), 956–958 (1986)
53. Cookson, D.J., E., S.B.: Atmospheric oxygen as the dominant source of ^{29}Si spin-lattice relaxation in solid silicalite. J. Magn. Reson. **63**, 217–218 (1985)
54. Koller, H., Lobo, R.F., Burkett, S.L., Davis, M.E.: SiO-HOsi hydrogen bonds in as-synthesized high-silica zeolites. J. Phys. Chem. **99**(33), 12588–12596 (1995)
55. Scarano, D., Zecchina, A., Bordiga, S., Geobaldo, F., Spoto, G., Petrini, G., Leofanti, G., Padovan, M., Tozzola, G.: Fourier-transform infrared and Raman spectra of pure and Al-, B-, Ti- and Fe-substituted silicalites: stretching-mode region. J. Chem. Soc. Faraday Trans. **89**, 4123–4130 (1993)
56. Decottignies, M., Phalippou, J., Zarzycki, J.: Synthesis of glasses by hot-pressing of gels. J. Mater. Sci. **13**(12), 2605–2618 (1978)
57. Soda, R.: Infrared absorption spectra of quartz and some other silica modification. B. Chem. Soc. Jpn. **34**(10), 1491–1494 (1961)
58. Hino, M., Sato, T.: Infrared absorption spectra of silica gel-$H_2{}^{16}O$, $D_2{}^{16}O$, and $H_2{}^{18}O$ systems. Bull. Chem. Soc. Jpn. **44**(1), 33 (1971)
59. Llewellyn, P.L., Coulomb, J.P., Grillet, Y., Patarin, J., Andre, G., Rouquerol, J.: Adsorption by MFI-type zeolites examined by isothermal microcalorimetry and neutron diffraction. 2. nitrogen and carbon monoxide. Langmuir **9**, 1852–1856 (1993)